

Fig. 4. Localization of GFP-ErbB fusion proteins. The columns labeled ErbB-4-GFP and GFP-ErbB-4 show GFP fusions at the COOH- or NH₂-terminus, respectively, of the ErbB-4 cytoplasmic domain (residues 676 to 1308); the right column shows GFP fusion at the NH₂-terminus of ErbB-2 (residues 676 to 1255). Fusions were constructed and expressed in COS-7 cells as described (17). After 48 hours, the cells were examined by confocal microscopy. The cells in the bottom panels were incubated for 1 hour with LMB (100 ng/ml) before microscopy. Scale bar, 25 μ m.

the nucleus and promote transcription after γ -secretase cleavage (12, 16). We have used the GAL4 transactivation system in COS-7 cells to assess the possible transactivation potential of the ErbB-4 cytoplasmic domain. The results indicate that the COOH-terminal domain of ErbB-4 has weak transcriptional activity (about three times that of the control GAL4 DNA binding domain), whereas the ErbB-4 kinase domain and the complete cytoplasmic domain have no increased activity relative to the control (17). When expressed as GFP fusion proteins, the ErbB-4 COOH-terminal domain localized to the nucleus, but the kinase domain was present mainly in the cytosol (17). Recently it was reported that the EGF receptor (ErbB-1) is localized to the nucleus and that its COOH-terminal domain functions as a transcription factor in several assays, including the GAL4 system (18).

HRG association with ErbB-4 inhibits growth and induces the differentiation of mammary carcinoma cell lines (19, 20). When serum-deprived T47D mammary carcinoma cells were treated with HRG, the total cell number decreased (Table 1). In contrast, treatment of the cells with EGF increased the cell number. Addition of the γ -secretase inhibitor compound E completely abrogated the HRG-induced cell loss but had no effect on the growth-stimulatory effect of EGF. This result indicates that γ -secretase activity is necessary for this biological response to HRG. HRG responses in T47D cells could involve ErbB-3 or ErbB-2 in addition to ErbB-4, but we have not detected proteolytic cleavage of ErbB-3 or ErbB-2 in these cells (5).

ErbB-4 is a receptor tyrosine kinase that is proteolytically processed by consecutive ectodomain and intramembrane cleavages, re-

sulting in the nuclear translocation of its cytoplasmic domain. Although ectodomain cleavage of several other receptor tyrosine kinases has been reported, it is not known whether any are also processed by γ -secretase activity. Because the s80 ErbB-4 fragment contains a tyrosine kinase domain, nuclear substrates may become phosphorylated by the s80 fragment, further extending the receptor's mechanism of action.

References and Notes

1. Y. Yarden, M. X. Sliwkowski, *Nature Rev. Mol. Cell Biol.* **2**, 127 (2001).
 2. M. Vecchi, G. Carpenter, *J. Cell Biol.* **139**, 995 (1997).

3. W. Zhou, G. Carpenter, *J. Biol. Chem.* **275**, 34737 (2000).
 4. C. Rio, J. D. Buxbaum, J. J. Peschon, G. Corfas, *J. Biol. Chem.* **275**, 10379 (2000).
 5. C.-Y. Ni, W. Zhou, G. Carpenter, unpublished data.
 6. M. S. Brown, J. Ye, R. B. Rawson, J. L. Goldstein, *Cell* **100**, 391 (2000).
 7. T. Hoppe et al., *Cell* **102**, 577 (2000).
 8. S. S. Bae et al., *FEBS Lett.* **491**, 16 (2001).
 9. C. McLendon et al., *FASEB J.* **14**, 2383 (2000).
 10. M. S. Shearman et al., *Biochemistry* **39**, 8698 (2000).
 11. D. Seiffert et al., *J. Biol. Chem.* **275**, 34086 (2000).
 12. H. Steiner, C. Haass, *Nature Rev. Mol. Cell Biol.* **1**, 217 (2000).
 13. M. P. Murphy et al., *J. Biol. Chem.* **275**, 26277 (2000).
 14. R. Srinivasan, C. E. Gillett, D. M. Barnes, W. J. Gullick, *Cancer Res.* **60**, 1483 (2000).
 15. Given that the nuclear export signal consensus sequence is XR₂₋₄XR₂XR₂X (where X represents Leu, Ile, or Val, and R represents any amino acid), there are three putative nuclear export signal sequences in the ErbB-4 cytoplasmic domain sequence: Leu⁷¹³-Lys-Glu-Thr-Glu-Leu-Lys-Arg-Val-Lys-Val-Leu, Leu⁷⁸⁰-Val-Arg-Leu-Leu-Gly-Val-Cys-Leu, and Leu⁹³⁹-Pro-Gln-Pro-Ile-Cys-Thr-Ile-Asp-Val.
 16. X. Cao, T. C. Sudhof, *Science* **293**, 115 (2001).
 17. For supplementary figures showing that the ErbB-4 COOH-terminal domain has activity in the GAL4 transactivation assay and is localized in the nucleus as a GFP fusion protein, see Science Online (www.sciencemag.org/cgi/content/full/1065412/DC1).
 18. S.-Y. Lin et al., *Nature Cell Biol.* **3**, 802 (2001).
 19. E. Peles et al., *Cell* **69**, 205 (1992).
 20. C. Sartor et al., *Mol. Cell Biol.* **21**, 4265 (2001).
 21. We thank H.-J. Liao, X.-J. Wang, and H.-P. Yuan for their help; A. Fauq and C. Ziani-Cherif for the synthesis of Y1L and compound E; M. Yoshida for LMB; M. Kraus for ErbB-4 antibody; M. Vecchi for GAL4 constructs; and O. Tikhomirov for the GFP-ErbB-2 construct. Supported by NIH grants CA24071 (G.C.) and NS39072 (T.E.G.) and by an Ellison Medical Foundation New Scholars award (T.E.G.). Core facility support from grants CA68485 (Vanderbilt-Ingram Cancer Center) and DK20593 (Vanderbilt Diabetes Center) is acknowledged.

14 August 2001; accepted 12 October 2001
 Published online 25 October 2001;
 10.1126/science.1065412

Include this information when citing this paper.

Chromosome Dynamics in the Yeast Interphase Nucleus

Patrick Heun,* Thierry Laroche, Kenji Shimada, Patrick Furrer,† Susan M. Gasser‡

Little is known about the dynamics of chromosomes in interphase nuclei. By tagging four chromosomal regions with a green fluorescent protein fusion to *lac* repressor, we monitored the movement and subnuclear position of specific sites in the yeast genome, sampling at short time intervals. We found that early and late origins of replication are highly mobile in G₁ phase, frequently moving at or faster than 0.5 micrometers/10 seconds, in an energy-dependent fashion. The rapid diffusive movement of chromatin detected in G₁ becomes constrained in S phase through a mechanism dependent on active DNA replication. In contrast, telomeres and centromeres provide replication-independent constraint on chromatin movement in both G₁ and S phases.

Most information available on the nuclear organization of chromosomes is based on the analysis of fluorescent probes in formaldehyde-fixed cells. It is generally assumed that

chromosomes, which occupy distinct "territories" in mammalian nuclei (1), are relatively static when compared to metaphase chromosomes. This notion of nuclear order is

REPORTS

supported by hybridization with specific DNA sequences: Centromeric heterochromatin is often found at the nuclear periphery or surrounding nucleoli, as are transcriptionally silent chromosomes, like the inactive X (2). In budding yeast, roughly 70% of telomeres (3) and late-firing origins (4) are positioned

University of Geneva, Department of Molecular Biology, Quai Ernest-Ansermet 30, CH-1211 Geneva, Switzerland.

*Present address: The Salk Institute, 10010 North Torrey Pines Road, La Jolla, CA 92037, USA.

†Present address: Euresearch, Effingerstrasse 19, 3001 Bern, Switzerland.

‡To whom correspondence should be addressed. E-mail: susan.gasser@molbio.unige.ch

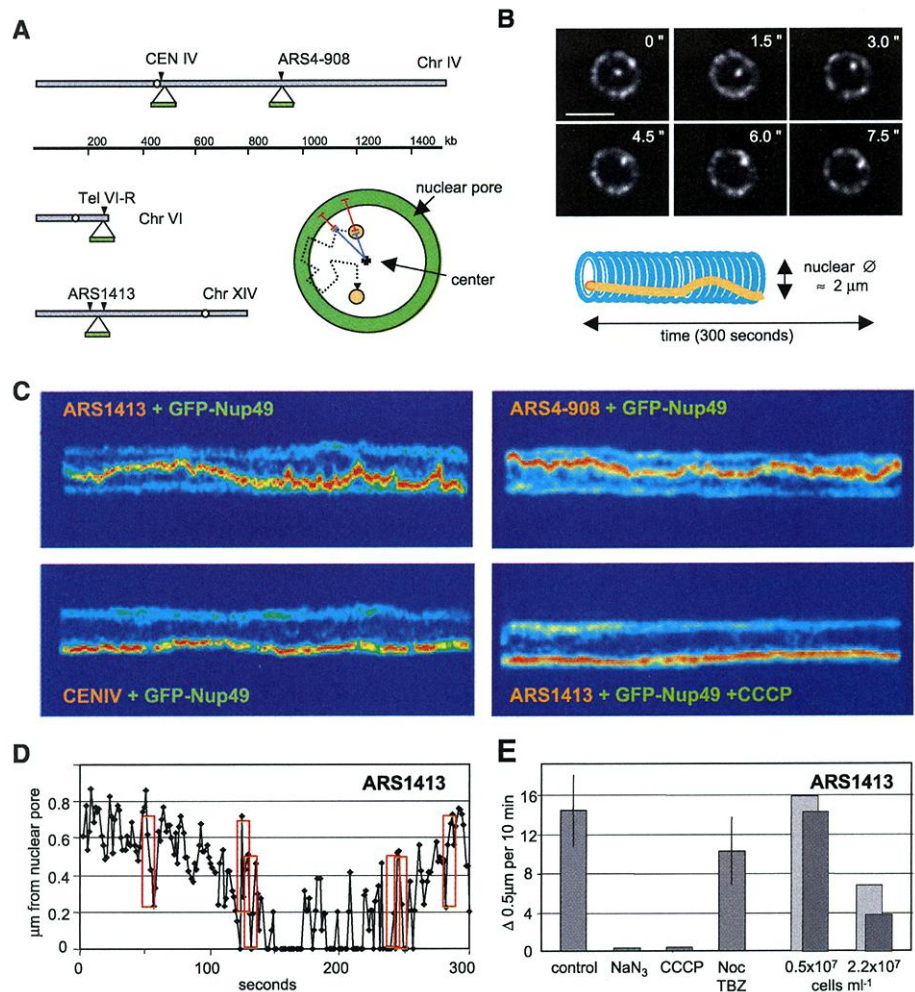
near the nuclear envelope in G_1 phase, with telomeres clustering in three to eight foci. Furthermore, using a green fluorescent protein (GFP)-tagged (5) centromere, relative movement between two homologous yeast chromosomes was measured, showing that centromere III is confined to a subnuclear zone of restricted radius ($\leq 0.25 \mu\text{m}$) (6).

Nonetheless, nuclear organization may not be as static as these studies suggest. In *Drosophila* larval nuclei, large chromosomal movements have been observed in early G_1 phase (7), and both large and small movements have been confirmed by real-time microscopy for a single locus in the premeiotic nuclei of fly spermatocytes (8). To examine

the dynamics of interphase chromatin in yeast, we exploited the *lac* operator-repressor interaction to detect four distinct chromosomal domains. The expression of a GFP-*lac* repressor fusion in cells that carry an integrated array of multimerized *lac* repressor binding sites (*lac*^{OP}) (5) allows the tracking of specific chromosomal sites by real-time fluorescence microscopy. By combining this with a GFP-tagged copy of a nuclear pore protein (Nup49p) to label the nuclear envelope (9), we can measure movements of the chromosomal DNA in relation to the nuclear periphery or the calculated center of the nuclear plane.

Here, we have integrated a single cluster

Fig. 1. Visualization of interphase chromatin movement in budding yeast. **(A)** Four chromosomal sites were tagged independently in a haploid *S. cerevisiae* strain that expresses a GFP-nuclear pore protein fusion (4) (Nup49-GFP^{S65T}). As shown, roughly 10 kb of tandemly repeated *lac*^{OP} consensus (5) were integrated within 15 kb of centromere CEN IV, early replicating origin ARS4-908 (4), telomere TEL VI R, and between two internal late firing origins ARS1412 and ARS1413 [labeled ARS1413 (4)]. Two methods are used to quantify the movements of the tagged chromosomal loci. After alignment of the nuclear pore signals through the time series, absolute movement of the spot is followed frame-by-frame (Fig. 3, Tracking). Alternatively, displacement of the spot is measured relative to either the nuclear periphery (red bars) or the nuclear center (blue bars). The center is calculated using a Metamorph program that defines an optimized circle based on the nuclear pore fluorescence [see details in supplementary methods (71)]. Spot-to-pore distance was measured manually using the Zeiss confocal LSM version 2.5 software. **(B)** Shown are six frames taken on a Zeiss LSM 510 confocal microscope (63 \times objective, zoom 3) at ~ 1.5 s intervals, showing the haploid G_1 phase nucleus of strain GA-1325, tagged at ARS4-908. The bright internal spot represents ARS4-908 and GFP-Nup49, labels the nuclear periphery. Bar, 2 [f_4] μm /[f_4] μm [see time-lapse movie at (71)]. Sequential images can be orthogonally displayed using the Zeiss 510 LSM software, and rotated such that the time axis (z) is displayed horizontally. **(C)** A 3D projection of 200 images (5 min) of the tagged locus ARS1413, ARS4-908, or CEN IV (yellow/red, as indicated) and nuclear pore (cyan) is shown for G_1 phase cells. Different intensities in fluorescence are shown in false color (highest is red, lowest blue). Where indicated, 40 mM CCCP was added 15 min before and during time-lapse microscopy. Standard imaging uses cells from a culture of a GFP-*lac*^{OP} tagged strain at $\sim 5 \times 10^6$ cells/ml, on slides coated with SD agar – histidine + 4% glucose. Time-lapse image capture during 5 min on a Zeiss LSM 510 (200 scans using total 0.5 s scanning time with 1 s pause; 100 \times Planapo objective and zoom 2 are used unless otherwise indicated). Time-lapse series are available at (71) for each locus studied. **(D)** Typical measurements of the distance from the center of the ARS1413 focus to the center of the closest GFP-Nup49 signal are plotted in nm from the pore. The plotted distances were scored for movements $\geq 0.5 \mu\text{m}$ that occur in under 10 s (examples boxed in red). The total number of large movements scored for each condition is then divided by the total time and expressed as movements per 10 min. **(E)** Summary



of large movement frequencies for ARS1413 under control conditions [1% dimethyl sulfoxide (DMSO)], 40 mM CCCP, 10 $\mu\text{g}/\text{ml}$ nocodazole and 300 $\mu\text{g}/\text{ml}$ thiabendazole (noc/TBZ), or 0.15 mM Na_3N for 15 min prior to and during time-lapse microscopy. Each value is derived from multiple time-lapse movies of different G_1 phase cells. Total minutes analyzed (40 images/min) are: control, 13.3 min; CCCP, 12.4 min; Noc+TBZ, 23.8 min; Na_3N , 19.4 min. The error bar indicates the range of values obtained with a 10% uncertainty of distance measurement (large movements monitored as either 0.45 μm or 0.55 μm). ARS1413 cells were also monitored as a function of culture saturation (cells ml^{-1}), and were scanned either in the presence (hatched bars) or absence (gray bars) of 4% glucose. Only mother cells are measured in all experiments (further details in Web fig. 2).

REPORTS

of 256 *lac^{OP}* sites into a haploid strain of *Saccharomyces cerevisiae* (GA-1320) either at a late-replicating region between two origins of replication (ARS1412 and ARS1413), located 240 kb from the left telomere of chromosome XIV, or near an early-activated origin on chromosome IV, 908 kb from the left telomere [ARS4-908 (4) (Fig. 1A)]. Both sites are within 10 kb of transcribed genes and the nearest origin of replication, and serve as examples of general chromatin structure. As markers for specialized chromosomal domains, we tagged one site 15 kb from the right end of chromosome VI, preserving the subtelomeric repeat structure (TEL VI R), and a second site 12 kb from the centromere of chromosome IV (CEN IV). The binding of GFP-*lac* repressor produces a bright spot of $\sim 0.3 \mu\text{m}$ in diameter (Fig. 1B), which can be readily distinguished from the more weakly fluorescent ring of the nuclear envelope ($\varnothing = 1.7$ to $2 \mu\text{m}$). Cell cycle stages are assigned by correlating the presence and the relative size of the bud, and nuclear size and shape, with DNA content, as detected by fluorescence-activated cell sorting analysis. Rapid capture of images by laser scanning microscopy (the nucleus is scanned within ~ 150 ms at 1.5 s repeat intervals) allows us to monitor the movement of these loci over a 5-min period at high resolution (10).

The bright foci representing either ARS4-

908 or ARS1413 are extremely dynamic in G_1 phase nuclei, showing two characteristic types of movement (Fig. 1B) [Web movies (11)]. In sequential frames, we observe both short fluctuations in position (distances $\leq 0.2 \mu\text{m}$) and, less frequently, larger movements ($\geq 0.5 \mu\text{m}$; Fig. 1D and Web fig. 1). We also observe deformations of the entire yeast envelope and oscillatory movements of pores within the nuclear membrane. If we project a series of 200 sequential 2D images horizontally, aligning the nuclear pore signals, we see that the dynamics of the tagged ARS1413 or ARS4-908 loci are distinct from overall nuclear movement or minor fluctuations in nuclear shape (compare bright yellow/red signal of the GFP *lac* repressor to cyan signals; Fig. 1, B and C). The movement of the tagged origins is not due to inanimate forces, because the addition of NaN_3 arrests this movement completely (Web fig. 2 and Fig. 1E). Importantly, an identical *lac^{OP}* tag inserted near CEN IV does not show equivalent motion (Fig. 1C).

By quantifying movements of the tagged chromosomal site relative to either the nearest point on the nuclear envelope or the center of the nuclear sphere calculated from the GFP pore signal, we eliminate any component of the movement that results from nuclear drift (Fig. 1, A and D). As a measure of large movements, we score for chromatin displacements

$\geq 0.5 \mu\text{m}$ that occur in less than 10 s (Fig. 1D, red boxes). Their frequency is averaged over multiple time-lapse series and is expressed as large movements per 10 min.

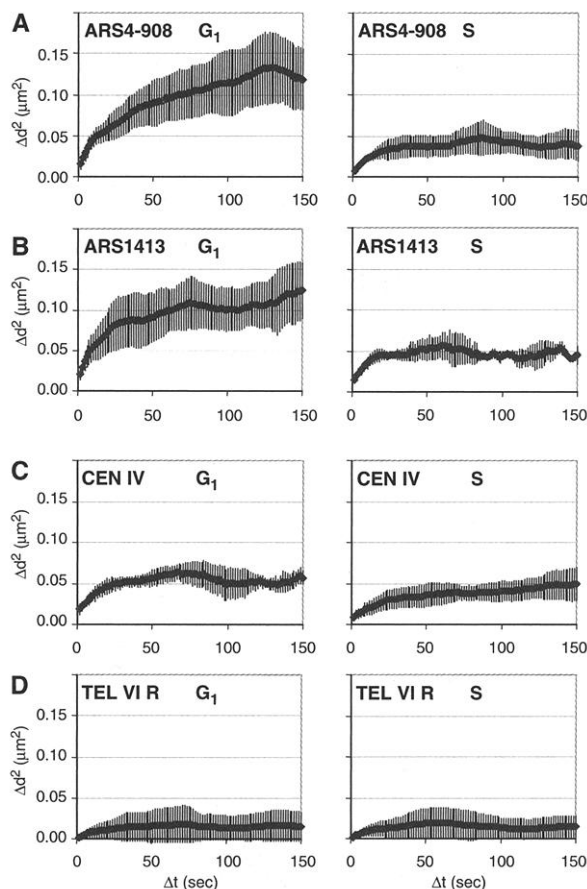
The dynamic chromatin behavior appears not to reflect simple Brownian motion, i.e., movement resulting from random indirect forces upon the chromosomal fiber, because exposure of yeast to carbonyl cyanide chlorophenyl hydrazone (CCCP), an uncoupler of the mitochondrial F_1F_0 adenosine triphosphatase, largely suppresses the movement (Fig. 1, C and E, and Web movie). This protonophore also collapses plasma membrane potential, reduces intracellular ATP levels, and arrests cell growth (12). On the other hand, the frequency of large movements is not altered by the presence of the microtubule-destabilizing drugs, nocodazole and thiabendazole (+ noc/TBZ, Fig. 1E) and is therefore unlikely to be mediated by microtubule-dependent motors.

To further correlate large chromatin movements in G_1 with the cell's metabolic status, ARS1413-*lac^{OP}* dynamics are followed as cell density increases in a growing culture. The frequency of $\geq 0.5 \mu\text{m}$ movements drops four-fold in G_1 phase as cell density increases, an effect enhanced when microscopy is monitored on glucose-depleted media (Fig. 1E, dark bars; Web fig. 2). The drop in mobility occurs at $\sim 2 \times 10^7$ cells/ml, or roughly one generation before the first changes in gene expression and chromatin structure that accompany the diauxic shift, a transition from fermentative and oxidative metabolism (13), suggesting that large-amplitude movements may correlate with intracellular ATP levels. The smaller, oscillatory movements are not abolished for ARS1413 and ARS4-908, even in stationary-phase cells.

It has been proposed that both centromeres and telomeres are clustered near the yeast nuclear periphery (3, 4). Consistently, our time-lapse analyses on cells bearing a GFP-tagged natural telomere (TEL VI R) or CEN IV (Fig. 1D) reveal an absence of large movements for both centromeric and telomeric tags, although smaller movements are readily detected at CEN IV (Web fig. 3 and Web movies). The telomere oscillates adjacent to the nuclear envelope, such that the distance from the tag to the nuclear pore rarely exceeds $0.3 \mu\text{m}$. Nonetheless, TEL VI R moves significantly more than an integral nuclear envelope component (see below, Fig. 3C). The constraint on telomere mobility persists through S phase until late G_2 phase, when the nucleus deforms to enter the daughter cell (14).

By scoring early S phase cells (shortly after bud emergence), we note that the large-amplitude movements of both tagged origins are significantly less frequent once cells enter S phase, although the smaller oscillatory movements continue (Web fig. 3). In con-

Fig. 2. Origins are less constrained than telomeres and centromeres in G_1 phase, but all sites show spatial constraint in S phase. Mean squared displacement analysis was performed as described (6, 8), by computing the square of the displacement of the indicated focus (measured from the center of the chromosomal tag to either the nuclear center or the nuclear periphery) in μm (Δd^2) as a function of the time interval Δt (s): $\Delta d^2 = \{d(t) - d(t + \Delta t)\}^2$ for Δt ranging from 1.5 to 150 s. The average of all Δd^2 values for each Δt value are plotted against Δt . The slope is the derivative of displacement or diffusion coefficient. The graphs represent averages from all movies available for each condition with standard deviation indicated. The number of nuclei and images analyzed for each phase areas follows: (A) G_1 : 10 nuclei / 2000 frames; S: 5 / 1000, (B) G_1 : 8 / 1600; S: 3 / 600, (C) G_1 : 4 / 800; S: 3 / 600, (D) G_1 : 3 / 600; S: 4 / 800.



REPORTS

trast, the amplitude of centromere movement remains unchanged between G_1 and S phase cells. To determine whether this suppression reflects a reduced confinement radius, we have calculated the mean squared displacement over time (MSQD), which was previously used to monitor spatial constraints on the relative movements of two homologous sites in diploid yeast (or fly cells) (6, 8). When the square of the displacement within discrete time intervals (ranging from 1.5 to 150 s) is plotted as a function of increasing time intervals (Δt), a monotonic increase would indicate unconstrained movement or free diffusion. A rapid increase followed by a plateau indicates that the movement is constrained within a limited area (or sphere), the radius of which can be estimated. By plotting the MSQD curves for each locus averaged over all available time intervals in either G_1 or S phase cells, we obtain a reliable estimate of each locus' degree of freedom.

Figure 2 presents the MSQD graphs averaged over multiple movies of each of the four chromosomal loci we have tagged [examples of each are at (11)]. The initial slope (i.e., diffusion coefficient) and plateau values for CEN IV (Fig. 2C) are remarkably similar to those previously reported for CEN III (6) ($0.05 \mu\text{m}^2$, indicating a radius of confinement $\leq 0.3 \mu\text{m}$). The curves and plateau values do not change significantly between G_1 and S phase for CEN IV and TEL VIR, whereas the radii of constraint calculated for ARS1413 and ARS4-908 are significantly lower in S than in G_1 phase. In G_1 , the biphasic curve increases until time intervals of 75 and 100 s, with a plateau at 0.1 to $0.15 \mu\text{m}^2$. A plateau at this value was previously shown (6) to correspond to a radius of confinement of roughly $0.7 \mu\text{m}$, or an occupied volume 10-fold larger than that of the yeast centromere or of origins in S phase (Fig. 2, A through C, panels S). The S-phase MSQD curves of ARS1413, ARS4-908, and CENIV are all similar, starting with a steep slope that arrives at a plateau of $\sim 0.05 \mu\text{m}^2$ (radii of confinement $\leq 0.3 \mu\text{m}$).

The displacement measurements shown above indicate changes in spatial constraints dependent on the cell cycle, but do not identify position within the nucleus. To visualize the localization and path length of a given tagged domain over 5 min, we align the nuclear pore signals of a given time-lapse series, and follow the path of the tagged locus from frame to frame with a tracking tool. The cumulative path (Fig. 3, in red) is then projected onto a single nuclear section. The sum of the vectors' lengths indicates a minimal linear distance (in μm) traveled within 300 s (15). By projecting the entire time-lapse series into one plane and calculating the surface area that encompasses the path, a value related to the radius of confinement is obtained

(Fig. 3, "Projection," and Web fig. 5).

Consistent with MSQD measurements, tracking confirms that the tagged origins move less in S phase than in G_1 (Fig. 3A). It also underscores the close association of TEL VIR with the nuclear envelope (3, 4). In addition, we see that the movements have no cumulative directionality (16) and that ARS4-908 and ARS1413 can "sample" large

areas of the nucleus within 5 min. These loci in G_1 phase cells have the least spatial constraint, whereas TEL VIR remains primarily juxtaposed to nuclear periphery. Our observations do not refute the notion of nuclear territories (1), yet they suggest that such territories are loosely defined in yeast, perhaps entailing only a few anchorage sites.

A mean linear trajectory for each locus

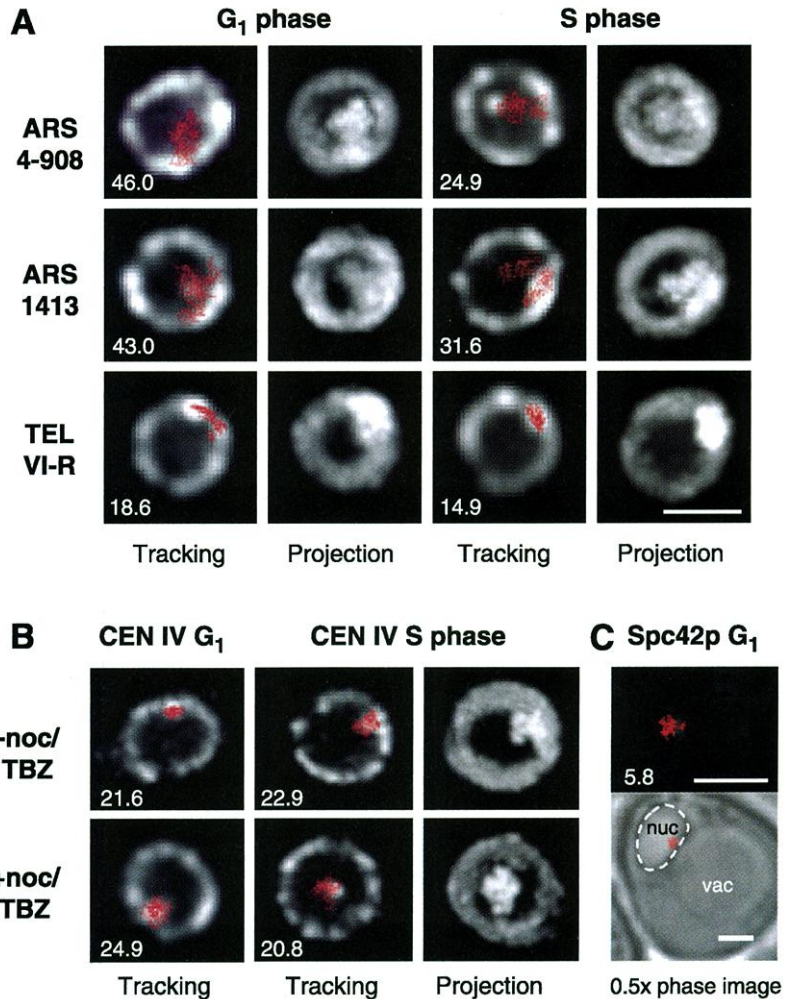


Fig. 3. TEL VIR and CENIV are constrained to perinuclear zones, while other loci have less restricted subnuclear positions. (A) Isogenic yeast strains carrying the indicated GFP-tagged locus and GFP-Nup49 were analyzed under standard conditions as described above, in G_1 and S phase. Nuclear pore signals were aligned for each time-lapse series and the position and total distance traveled by the indicated tag was measured using the AIM tool of the Zeiss LSM 510 software (release 2.8). The trajectory over 300 s (in red), is superimposed on a single nuclear focal section (Tracking). The mean length of the path in μm averaged over four or five movies is indicated, and standard deviations range from less than $1 \mu\text{m}$ (for TEL VIR) to $8 \mu\text{m}$ (ARS4-908). An intensity projection of the same stack of images is shown (Projection), and the area occupied by the accumulated signal covers on average $30 \pm 4\%$ ($n = 10$) of the nuclear surface for ARS1413 and ARS4-908 in G_1 and $20 \pm 5\%$ ($n = 8$) in S phase. TEL VIR occupies $10\% [\pm 3\%]$ ($n = 4$). (B) Tracking and trajectory measurement are shown for CEN IV in G_1 and S phase cells, either in the presence of DMSO alone, or with nocodazole and thiabendazole (\pm noc/TBZ; Fig. 1). The amplitude and average path length changes little from G_1 to S, although destabilization of microtubules shifts CEN IV internally in some S-phase nuclei. Trajectory distances are given in μm ($n = 4$ for S phase, $n = 1$ for G_1). (C) Time-lapse microscopy and tracking was performed for a CFP-tagged spindle pole body component, Spc42p (17). Because Spc42p is in the nuclear envelope, we trace its movement with respect to the transmitted light image of the cell. The upper image is on the same scale as all other tracking images, while the lower transmitted light image of the entire cell is half this magnification. A white dotted line encircles the nucleus (nuc) and vac, the vacuole. Bars, $2 \mu\text{m}$. The average of Spc42p trajectory length is $5.8 \pm 1.2 \mu\text{m}$ ($n = 3$).

was calculated on the basis of multiple 5-min movies and is indicated in each panel (Fig. 3). Although TEL VIR remains close to the nuclear envelope, it moves three times the distance of an integral component of the nuclear envelope, a 42 kD spindle pole body protein (17) (Fig. 3, A and C), indicating that at least one aspect of telomere movement is independent of the nuclear envelope. Exposing S phase cells to microtubule depolymerizing agents provokes a more frequent migration of CEN IV to the interior of the nucleus, but does not significantly increase the amplitude of its movement (Fig. 3B, + noc/TBZ), although nocodazole does not alter the position or amplitude of movement for the other tagged loci in G₁ or S phase (Fig. 1E) (18).

To see if the S phase–specific restriction on the dynamics of ARS1413 and ARS4-908 is a direct effect of DNA replication, we inhibited DNA synthesis by the addition of hydroxyurea (HU), which depletes dNTP pools, or by aphidicolin, a specific inhibitor of DNA polymerase elongation. As expected, in control cells, the frequency of large-scale movements drops between G₁ and S phase. Importantly, when S-phase cells are treated with the inhibi-

tors, large movements of both ARS1413 and ARS4-908 are again as frequent as in G₁ (Fig. 4A). Neither the loading of the MCM complex by the origin recognition complex (ORC) and Cdc6p, nor its release by initiation, is likely to be the stabilizing factor in S phase, because this assembly occurs in G₁, and MCM release does not occur for late-firing origins like ARS1413 in HU (19). Besides arrest fork movement, treatment with either HU or aphidicolin activates the DNA checkpoint pathway (20). However, because the increase in S-phase dynamics in HU occurs in a *rad53* mutant (Fig. 4A), it is unlikely to be related to a checkpoint response.

In yeast, as in higher eukaryotes, each replication fork is predicted to assemble a complex of ~2000 kD, and multiple such complexes appear to aggregate at sites of replication (21). If such assemblies are sufficient to impede chromatin mobility, then constraint should reflect the number of active replication forks. This was tested by monitoring relative G₁ and S phase mobility in a strain carrying the yeast *orc2-1* deficiency. This mutation confers a significant drop in the efficiency of origin firing (22) and a reduction in replication foci formation (23),

even at 23°C, by destabilizing the conserved six-subunit ORC (22, 24). Indeed, when monitored for large chromatin movements of ARS1413, the *orc2-1* mutant cells lose the suppression normally detected in S phase at either 23° or 30°C (Fig. 4B). Tracking data confirm that the distances moved by the tagged ARS1413 in the *orc2-1* mutant in G₁ and S phases at 30°C are identical, whereas in isogenic ORC2 cells, the linear trajectory decreases by ~25% in S phase (25).

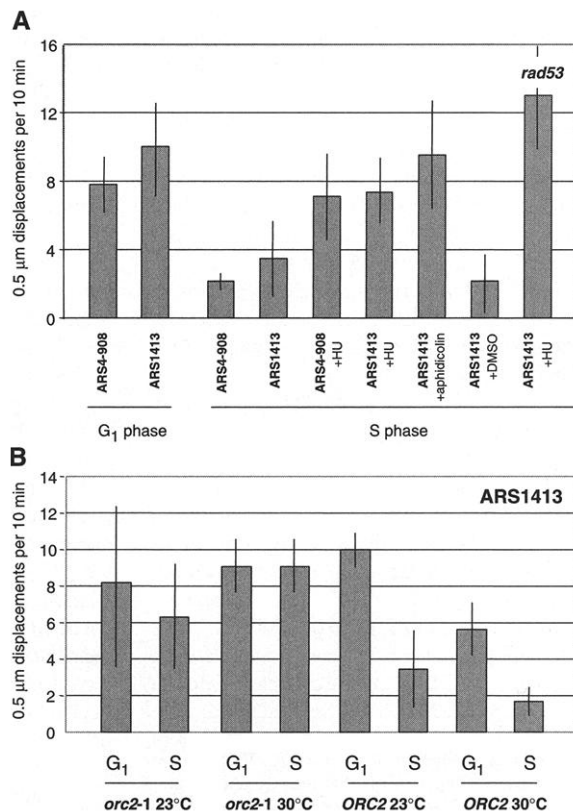
We have documented a highly dynamic behavior of interphase chromatin in yeast, which moves distances ≥0.5 μm within seconds. We establish that movements detected for different chromosomal domains have different degrees of constraints. Telomeres move significantly less than other regions, consistent with previous data suggesting that they are tethered to the nuclear periphery (3, 4). The amplitude of movement of nontelomeric chromatin appears to be modulated by both the metabolic status of the cell and DNA replication. This could either indicate that the viscosity of the nucleoplasm changes with the cell cycle or that the movement is propelled by an active mechanism, whose activity fluctuates. Alternatively, large replication complexes may impose additional sites of anchorage in S phase. The limited movement reported for interphase chromatin in the mammalian cells may reflect the scale on which such events have been previously monitored (1, 26). Whereas a movement of 0.6 μm covers nearly a third the diameter of the haploid yeast nucleus, it is only 1/30 of the diameter of a typical human cell nucleus (average Ø = 15 to 20 μm). Given the speed of these movements, extremely rapid detection is required to accurately score the position of the tag.

Nonetheless, the dynamics scored here in G₁ phase nuclei may be a universal characteristic of open chromatin (27), which constitutes 80 to 90% of the yeast genome. The constant sampling of local environment achieved by this movement may help regulate macromolecular interactions, as well as long-range sequence searching, like that associated with homologous recombination, which is particularly efficient in yeast. The apparent energy-dependence of the movement may implicate ATP-dependent enzymes, such as RNA polymerases or chromatin remodeling complexes in chromatin dynamics.

References and Notes

1. T. Cremer et al., *Cold Spring Harbor Symp. Quant. Biol.* **58**, 777 (1993); M. Dundr, T. Misteli, *Biochem. J.* **356**, 297 (2001).
2. N. L. Mahy, W. A. Bickmore, T. Tumber, A. S. Belmont, in *Chromatin Structure and Gene Expression*, S. C. R. Elgin, J. L. Workman, Eds. (Frontiers in Molecular Biology, Oxford Univ. Press, ed. 2, Oxford, 2000); J. M. Bridger, S. Boyle, I. R. Kill, W. A. Bickmore, *Curr. Biol.* **10**, 149 (2000).
3. M. Gotta et al., *J. Cell Biol.* **134**, 1349 (1996); W. H. Tham, J. S. B. Wyithe, P. K. Ferrigno, P. A. Silver, V. A. Zakian, *Mol. Cell* **8**, 189 (2001).

Fig. 4. Constraint of origin movement in S phase requires active DNA replication. (A) The number of large movements (≥ 0.5 μm) for ARS1413 or ARS4-908 has been quantified as in Fig. 1E, in G₁- and S-phase nuclei, with addition of 2% DMSO ± 0.2 M hydroxyurea (HU) or 500 μg/ml aphidicolin. Here, we indicate for each condition the site of the lac^{OP} tag, host cell genotype, cell cycle phase, the number of movies analyzed and total time in minutes: GA-1325 (ARS4-908/wild type, G₁: 10, 74.2; S: 5, 32.5), GA-1323 (ARS1413/wild type, G₁: 8, 59.9; S: 3, 14.4), GA-1325 (ARS4-908/wild type, S + HU: 5, 49.4), GA-1323 (ARS1413/wild type, S + HU: 9, 55.9), GA-1323 (ARS1413/wild type, S + aphidicolin: 3, 19.9), GA-1323 (ARS1413/wild type, S + 2% DMSO: 2, 14), GA-1588 (ARS1413/*mec2-1* (20) (= *rad53*), S: 6, 36.9). (B) Cultures of isogenic ORC2⁺ (GA-1323) or *orc2-1* mutant cells (GA-1591) carrying the ARS1413 tag, were grown at 23°C, to 0.5 × 10⁶ cells ml⁻¹. Time-lapse microscopy was done on half of the culture at 23°C, while half was shifted to 30°C for 30 min and analyzed at 30°C. Center of focus to nuclear center measurements were performed using Metamorph (Universal Imaging Corporation) (17). Large movements were calculated as above, but in this experiment, G₁ daughter cells were not excluded from analysis. The ±10% confidence levels are indicated as in Fig. 1E, except for *orc2-1* at 23°C, in which ±5% variation is shown (25). Indicated here for each strain is the number of cells, and total imaging time in min: GA-1591/*orc2-1* (G₁/23°C: 3, 11; S/23°C: 3, 22.1), GA-1591/*orc2-1* (G₁/30°C: 5, 36.5; S/30°C: 3, 21.7), GA-1323/ORC2⁺ (G₁/23°C: 4, 38.3; S/23°C: 3, 14.4), GA-1323/ORC2⁺ (G₁/30°C: 3, 21.8; S/30°C: 4, 29.8).



Negative Regulation of Neural Stem/Progenitor Cell Proliferation by the *Pten* Tumor Suppressor Gene in Vivo

Matthias Groszer,^{1,2,4} Rebecca Erickson,²
Deirdre D. Scripture-Adams,⁵ Ralf Lesche,^{1,2*} Andreas Trumpp,⁷
Jerome A. Zack,^{5,6} Harley I. Kornblum,^{2,3} Xin Liu,^{2,4†}
Hong Wu^{1,2†}

The mechanisms controlling neural stem cell proliferation are poorly understood. Here we demonstrate that the PTEN tumor suppressor plays an important role in regulating neural stem/progenitor cells in vivo and in vitro. Mice lacking PTEN exhibited enlarged, histoarchitecturally abnormal brains, which resulted from increased cell proliferation, decreased cell death, and enlarged cell size. Neurosphere cultures revealed a greater proliferation capacity for tripotent *Pten*^{-/-} central nervous system stem/progenitor cells, which can be attributed, at least in part, to a shortened cell cycle. However, cell fate commitments of the progenitors were largely undisturbed. Our results suggest that PTEN negatively regulates neural stem cell proliferation.

The *Pten* tumor suppressor gene encodes the first phosphatase frequently mutated somatically in various human cancers, including glioblastoma (1). Besides carcinogenesis, *Pten* may play important roles in brain development, as suggested by its ubiquitous central nervous system (CNS) expression pattern in embryos (2, 3) as well as by neurological disorders associated with PTEN germ-line mutations in humans (4). However, the early embryonic lethality of conventional *Pten*^{-/-} mice (5, 6) has precluded further studies of PTEN function during brain development.

To explore PTEN's role in early brain development, we generated a conditional *Pten* knockout mouse by flanking exon 5, encoding the phosphatase domain of PTEN, with *loxP* sequences (*Pten*^{loxP}) (Fig. 1A). *Pten*^{loxP/loxP} females were crossed with males carrying a nestin promoter-driven *Cre* transgene (*Cre*^{+/-}) that is activated in CNS stem/progenitor cells at embryonic day (E) 9 or 10, resulting in almost complete gene deletion in the CNS by mid-gestation (7, 8). In *Pten*^{loxP/+}; *Cre*^{+/-} mice, *Cre*-mediated deletion of the *loxP* allele ($\Delta 5$) was detectable in all neural tissues examined (Fig. 1B, lanes 1 to 5). To ensure complete deletion

of *Pten*, we generated *Pten*^{loxP/ $\Delta 5$} ; *Cre*^{+/-} mice carrying a conventional exon 5 deleted allele (*Pten* ^{$\Delta 5$}) and a *Pten*^{loxP} allele. No PTEN protein could be detected in the mutant brain (Fig. 1C), indicating nearly complete *Pten* deletion. *Pten* deletion leads to hyperphosphorylation of Akt and S6 kinase, known downstream effectors of phosphatidylinositol 3-kinase (Fig. 1C) that have been implicated in neuron survival and cell cycle control (9).

Examination of the *Pten*^{loxP/ $\Delta 5$} ; *Cre*^{+/-} brain revealed a marked increase in brain size (Fig. 1D). Measurements taken at E14, E18, and P0 (birth) demonstrated continuous increases in brain weight and in the ratio of brain weight to body weight (Fig. 1E, upper panels). P0 mutant brain weight and cell number were double those of wild-type controls (Fig. 1E, upper and lower left), a difference much greater than that seen in mice overexpressing BCL-2 (10) or in mice lacking p27 (11). Because deletion of *Drosophila* PTEN led to increased S6 kinase activity and enlarged cell size, we measured the cell size distribution in mutant brains by flow cytometry. Cells from *Pten*^{-/-} brains were larger than those of controls (Fig. 1E, lower right), providing evidence that PTEN regulates cell size in mammals.

Mutant mice were born with open eyes (Fig. 1D) and died soon after birth. Histological analyses of newborn mutant brains showed a proportional increase in overall brain structures, with no signs of hydrocephalus (Fig. 2A). In the brainstem, nuclei in mutant animals were not easily identifiable (Fig. 2B). It is unclear whether specific nuclei, such as CN7n (arrow), were missing or

- P. Heun, T. Laroche, M. K. Raghuraman, S. M. Gasser, *J. Cell Biol.* **152**, 385 (2001).
- C. C. Robinett *et al.*, *J. Cell Biol.* **135**, 1685 (1996); A. F. Straight, A. S. Belmont, C. C. Robinett, A. W. Murray, *Curr. Biol.* **6**, 1599 (1996).
- W. F. Marshall *et al.*, *Curr. Biol.* **7**, 930 (1997).
- A. K. Csink, S. Henikoff, *J. Cell Biol.* **143**, 13 (1998).
- J. Vazquez, A. S. Belmont, J. W. Sedat, *Curr. Biol.* **11**, 1227 (2001).
- N. Belgareh, V. Doye, *J. Cell Biol.* **136**, 747 (1997).
- In order to maximize the speed of image capture, we scan one focal section of the nuclear sphere every 1.5 s, and, if necessary, we adjust the objective between scans to keep the GFP-repressor spot in focus. The time required to capture lac^{CP} signal is ~15 ms, and the entire nucleus requires <150 ms. We analyse movies in which the plane of focus stays within a 1 μ m midsection of the nucleus, or roughly half the nuclear depth. To ensure that cell cycle progression is not disturbed as a consequence of light damage, bud emergence and division of the scanned cell are followed by transmission microscopy.
- Supplementary material is available at www.sciencemag.org/cgi/content/full/294/5549/2181/DC1.
- P. K. Hanson, J. W. Nichols, *J. Biol. Chem.* **276**, 9861 (2001); P. Heun, S. M. Gasser, data not shown.
- J. L. DeRisi, V. R. Iyer, P. O. Brown, *Science* **278**, 680 (1997); L. Rubbi *et al.*, *Biochem. J.* **328**, 401 (1997).
- T. Laroche, P. Heun, S. M. Gasser, unpublished observations.
- Because the contribution from movement in z is not available from our analysis, this is a minimal distance and true velocities cannot be determined.
- Statistical analysis suggests that sequential vector direction is not entirely random, although tracking shows that movement is not unidirectional. The nature of the constraints are under study (M. Blaszczyk, S. M. Gasser, unpublished observations).
- A. D. Donaldson, J. V. Kilmartin, *J. Cell Biol.* **132**, 887 (1996).
- P. Heun, T. Laroche, S. M. Gasser, data not shown.
- V. Levenson, J. L. Hamlin, *Nucleic Acids Res.* **21**, 3997 (1993); C. Santocanale, J. F. Diffley, *Nature* **395**, 615 (1998).
- S. Kim, T. A. Weinert, *Yeast* **13**, 735 (1997).
- S. M. Jazwinski, G. M. Edelman, *J. Biol. Chem.* **259**, 6852 (1984); D. Coverley, R. A. Laskey, *Annu. Rev. Biochem.* **63**, 745 (1994).
- S. P. Bell, R. Kobayashi, B. Stillman, *Science* **262**, 1844 (1993); M. Foss, F. J. McNally, P. Laurensen, J. Rine, *Science* **262**, 1838 (1993); J. J. Li, I. Herskowitz, *Science* **262**, 1870 (1993); C. Liang, M. Weinreich, B. Stillman, *Cell* **81**, 667 (1995).
- P. Pasero, D. Braguglia, S. M. Gasser, *Genes Dev.* **11**, 1504 (1997).
- K. Shimada, S. M. Gasser, unpublished observations. The *orc2-1* mutation reduces the number of origins that fire each cell cycle, yet the defect can be suppressed in a dose-dependent manner by overexpressing *orc2-1p*.
- Cell-to-cell variability of large movements is aggravated by the irregular shape of *orc2* nuclei, which increases error in Metamorph-based distance measurements, based on calculating the center of the nucleus. This variability, however, is not present in trajectory measurements.
- R. D. Shelby, K. M. Hahn, K. F. Sullivan, *J. Cell Biol.* **135**, 545 (1996); D. Zink *et al.*, *Hum. Genet.* **102**, 241 (1998); E. M. Manders, H. Kimura, P. R. Cook, *J. Cell Biol.* **144**, 813 (1999).
- P. Buchenau, H. Saumweber, D. J. Arndt-Jovin, *J. Cell Biol.* **137**, 291 (1997); T. Tsukamoto *et al.*, *Nature Cell Biol.* **2**, 871 (2000); T. Tumber, A. S. Belmont, *Nature Cell Biol.* **3**, 134 (2001).
- We thank P. Pasero, A. Taddei, and K. Dubrana for comments on the text, F. Neumann for tagging TEL VIR, and the Swiss Institute for Experimental Cancer Research, the Swiss Cancer League, and the Swiss National Science Foundation for support. Boehringer Ingelheim and Roche Research Foundation provided for fellowships to P.H., and IARC to K.S.

¹Howard Hughes Medical Institute, ²Department of Molecular and Medical Pharmacology, ³Department of Pediatrics, ⁴Department of Pathology and Laboratory Medicine, ⁵Department of Medicine and AIDS Institute, ⁶Department of Microbiology and Molecular Genetics, UCLA School of Medicine, Los Angeles, CA 90095, USA. ⁷Institut Suisse de Recherche Expérimentale sur le Cancer, Ch. de Boveresses 155, 1066 Epalinges/Lausanne, Switzerland.

*Present address: Epigenomics AG, Kastanienallee 24, 10435 Berlin, Germany.

†To whom correspondence should be addressed. E-mail: xliu@mednet.ucla.edu, hwu@mednet.ucla.edu

14 August 2001; accepted 11 October 2001